Analysis of nonlinear deformations and damage in CFRP textile laminates

Analysis of nonlinear deformations and damage in CFRP textile laminates

H. ULLAH[1], A.R. HARLAND[1], T. LUCAS[2], D. PRICE[2], V.V. SILBERSCHMIDT[1]

[1] Wolfson School of Mechanical and Manufacturing Engineering, Loughborough University, Leicester-shire, LE11 3TU, UK

[2] Adidas AG, Herzogenaruch, Germany

E-mail: H.Ullah@lboro.ac.uk

Abstract. Carbon fibre-reinforced polymer (CFRP) textile composites are widely used in aerospace, automotive and construction components and structures thanks to their relatively low production costs, higher delamination and impact strength. They can also be used in various products in sports industry. These products are usually exposed to different in-service conditions such as large bending deformation and multiple impacts. Composite materials usually demonstrate multiple modes of damage and fracture due to their heterogeneity and microstructure, in contrast to more traditional homogeneous structural materials like metals and alloys. Damage evolution affects both their in-service properties and performance that can deteriorate with time.

These damage modes need adequate means of analysis and investigation, the major approaches being experimental characterisation, numerical simulations and microtomography analysis. This research deals with a deformation behaviour and damage in composite laminates linked to their quasi-static bending. Experimental tests are carried out to characterise the behaviour of woven CFRP material under large-deflection bending. Two-dimensional finite element (FE) models are implemented in the commercial code Abaqus/Explicit to study the deformation behaviour and damage in woven CFRP laminates. Multiple layers of bilinear cohesive-zone elements are employed to model the onset and progression of inter-ply delamination process. X-ray Micro-Computed Tomography (MicroCT) analysis is carried out to investigate internal damage mechanisms such as cracking and delaminations. The obtained results of simulations are in agreement with experimental data and MicroCT scans.

1. Introduction

Woven-fabric composite laminates offer a number of attractive properties compared to their unidirectional-tape counterparts such as lower production costs, better drapability, good resistance to fracture and transverse rupture due to weaving resistance, and high impact strength [1, 2]. These properties have attracted the sports industry looking at their possibility to incorporate textile CFRP laminates in the design of sports products. Such products could be subjected to large-deflection bending and multiple impacts in service conditions. These loads generate high local stresses and strains leading to complex damage modes due to heterogeneity and anisotropy of composite laminates.

In a bending scenario, a laminate experiences transverse shear and normal stresses resulting in the interlaminar delamination damage, because of their low through-thickness strength and stiffness [3]. Damage evolution results in significant reduction of in-service mechanical properties and can lead to loss of structural integrity of the composite sports products with time.

Computational damage modelling of delamination requires the capability to model initiation and progression of damage. Delamination initiation in composite laminates is usually assessed by strength-based criteria; for instance, the maximum nominal stress, and quadratic strength criteria are used successfully for this purpose. Several techniques based on fracture-mechanics approach are employed in the finite element method (FEM) to simulate a delamination growth such as the J-integral, the virtual crack extension method and the virtual crack closure technique (VCCT) [4]. Fracture-mechanics analysis is limited in this respect since it neglects material's nonlinearity and requires the position of delamination crack to be known in advance [5]. A promising approach to model the material as well as geometric nonlinearities is to employ cohesive elements at the interface between the composite laminas. Cohesive-zone elements are based on the model proposed by Dugdale [6], who introduced the concept that stresses in the material are limited by the yield stress and that a thin plastic zone is generated in front of the crack. Cohesive-zone elements are able to predict both the onset and growth of delamination combining the strength- and fracture-based approaches in a single finite-element model without preliminary knowledge of a crack's location and propagation direction [7]. However, application of cohesive-zone elements to model progressive delamination in composite structures poses numerical difficulties related to the proper definition of stiffness of the interface layer, the requirement of highly refined finite-element meshes, and convergence difficulties associated with a softening behaviour of the interface material [8].

Damage such as delamination and cracking in composites laminates usually occur inside the laminates and is barely visible. Non-destructive evaluation (NDE) methods are required to visualise this three-dimensional (3D) internal deformation and damage behaviour of composite structures. One of the recent methods is Micro-Computed Tomography (MicroCT) that can be used for imaging of materials's internal structure based on X-ray absorption, which is related to the material density [9]. This technique has been used to investigate micro cracking and delamination in composite laminates at micron-range level [10, 11]. Badel *et al*. [12] found good behavioural correlation between the results obtained from simulations and MicroCT scans of deformed and undeformed woven glass and carbon fabric laminates.

Quasi-static and dynamic bending of composite laminates results in complex damage mechanisms, in which multiple delaminations and interfacial fractures are dominant ones. Damage initiation and growth in composite structures subjected to bending have been studied by numerous researchers, using various FE models [13-15]. However, these models are usually developed in the context of a static or steady-state crack propagation using implicit FE tools. Therefore, a further research work is needed to develop reliable FE models capable of simulating the damage progression behaviour of laminated composites under large-deflection bending loads resulting in more rational and optimised designs. However, these high-fidelity simulations of discrete damage mechanisms in composites need validation by NDE techniques such as MicroCT. To address these problems, this paper presents an efficient numerical simulation of interlaminar damage propagation in woven CFRP laminates under transverse loading, using a cohesive-zone element method.

2. Experimental tests

Experimental tests were conducted on two types 0°- and 90°- CFRP specimens under three-point bending conditions to obtain material properties and validate numerical models. The specimens were fabricated from a carbon-fibre fabric woven in 2/2 twill reinforcement in thermoplastic polyurethanes (TPU) polymer with a fibre volume fraction of 45%; the fabric has the same number of yarns in the warp and weft directions. Quasi-static flexural tests were carried out at indenter speed of 100 mm/min

using the Instron 5569 machine in accordance with the ISO 178 Standard. Five samples per orientation were tested under large-deflection bending until their ultimate fracture.

Both 0° and 90° CFRP samples exhibited a brittle failure response in flexure as shown in figure1. The tests resulted in the same flexural modulus of 44.7 GPa and ultimate flexural strengths of 833 MPa and 824 MPa for 0° and 90°, respectively. This similarity is due to the symmetry of fibres in both warp and weft directions in both types of samples. Stiffness degradation due to internal cracks and delamination occurs in 0° sample at about 80% of the ultimate load, where as 90° sample show no stiffness reduction before ultimate fracture. Although the samples undergo cracking and interlaminar damage before the structure loses its load-carrying capacity, the development of such inter-ply delamination is not reflected in the stress-strain diagram, i.e. the effect of these usually hidden and barely visible damage mechanisms is small. The elastic flexural modulus such as E_{11} and E_{22} are calculated from the mechanical tests of 0° and 90°, respectively, and listed in Table 1. Rest of the elastic properties in Table 1 are taken from [16], where a similar CFRP textile laminate has been studied.

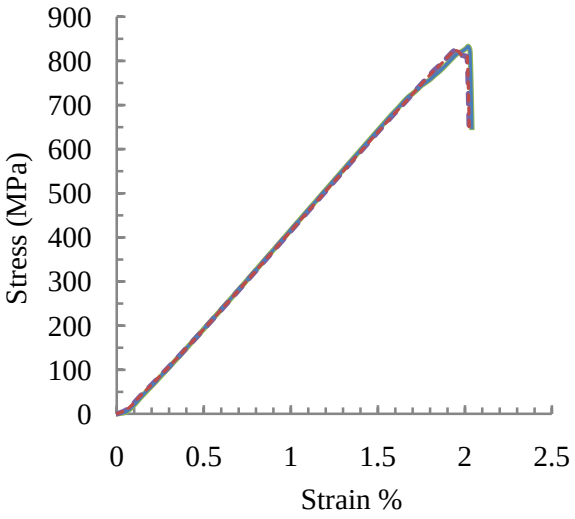

Figure 1. Stress-strain diagram from flexural tests of twill 2/2 CFRP

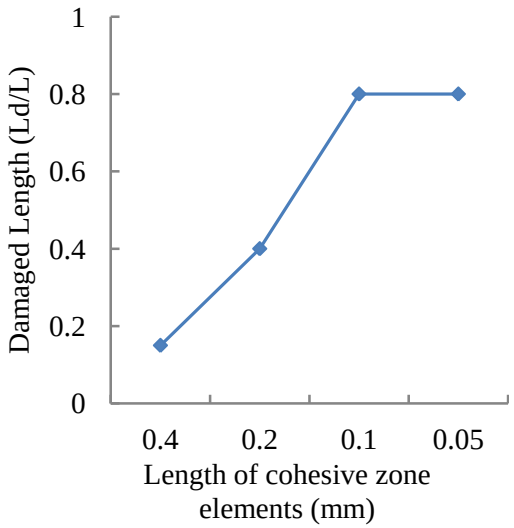

Figure 2. Damage sensitivity to cohesive element size

3. Finite-element modelling

Failure prediction of fibre-reinforced composite laminates is complicated by their heterogeneous nature, which gives rise to various types of multiple cracks, interacting strongly as failure progresses. Design and certification of most composite structures are based on empirical approaches because of the difficulty of comprehensive prediction of the damage process, with relatively little use of simulations. Therefore, there is a need for models, which are capable of simulating the entire damage process from its initiation through evolution to complete failure of a composite structure. The most promising tool is a computational approach based on the finite element method (FEM). However, the development of a proper numerical model representing the physics of damage mechanisms is a challenging task [17]. In this study, various approaches are implemented in finite-element models to characterise the onset and progression of damage for analysis of composite structures. The studies involve monitoring of a particular type of parameter such as stiffness degradation to predict the damage growth.

3.1. Modelling strategy

Finite element models are developed in the commercial FE package ABAQUS/Explicit to investigate large-deflection bending of tested composite laminates and the resulting interlaminar damage. Two FE models A and B are developed representing the bending tests on CFRP laminates. Model A contains two cohesive layers – one above the beam's neutral axis (NA) and the second coinciding with it, whereas model B has three interface layers - above, on and below the NA to simulate multiple delamination scenarios. The cohesive layer above the NA is referred to as top cohesive layer (TCL), the cohesive layer on the NA is referred to as mid cohesive layer (MCL) and the one below the NA is referred to as bottom cohesive layer (BCL). Theoretically, many interlaminar layers may be included in the model since the location of damage initiation is not known *a priori*. However, in such a case, the modelling effort, complications that are relevant to calibration of the penalty stiffness, and the computational time may increase, and the solution convergence becomes rather complicated. Furthermore, the number of cohesive layers in FE models should be such that the structure may be able to carry the applied load without losing its global stiffness before the damage starts in the actual laminate. In this three - point bending case, the cohesive layers are defined to simulate mixed-mode fracture mechanisms.

Table 1. Material properties of CFRP considered in the FE model

Elastic property		Interlaminar strength	and toughness
$E_{11} = E_{22}$ (GPa)	44.7	σ_{I0} (MPa)	12
G_{12} (GPa)	4.4	σ_{II0} (MPa)	26
ν_{12}	0.05	G_{Ic} (J/m^2)	800
E_{33} (GPa)	8.0	G_{IIc} (J/m^2)	1750
$G_{13} = G_{23}$ (GPa)	3.0		
$\nu_{13} = \nu_{23}$	0.3		

Since the laminate has a considerable length in z-direction, two-dimensional FE models based on plane-strain elements are developed to represent out-of-plane bending behaviour in a computationally cost effective manner. Composite laminas are meshed with plane-strain reduced-integration and hourglass-control CPE4R elements capable of eliminating the shear locking in bending problems, using the structured meshing technique. Interlaminar cohesive layers are meshed with two-dimensional COH2D4 elements using sweep mesh control. Indenter load application is represented by a circular rigid arc at the centre of the beam that is also laterally supported by two other circular rigid arcs. Surface-to-surface explicit contact is defined between the rigid arcs and the laminate top and bottom surfaces. All composite laminas are assigned elastic properties shown in Table 1. Interlaminar strengths and fracture toughness are indentified by numerical analyses. Normal σ_{I0} and shear σ_{II0} strengths are calibrated from the FE analysis of the undamaged beam under the same boundary conditions. In the FE analysis, the interlaminar shear stress is recorded as the interlaminar shear strength of the composite laminate at the failure observed in the experimental tests of CFRP laminate, employing the approach in [18]. Similarly, normal stress at the ultimate load is taken as the normal strength of the laminate. The fracture toughness in mode I G_{Ic} and mode II G_{IIc} are determined based on numerical optimisation in a way that the corresponding FE model was capable to represent damage in the bending test of the laminate.

3.2. Multiple delamination modelling using cohesive-zone elements

Computational models with the capability to predict the initiation and progression of delaminations can reduce the number of costly experimental tests and can lead to improved designs. Cohesive-zone elements (CZE) have the ability to capture the onset and propagation of delamination [8, 16]. Cohesive elements can be defined at various locations in FE models, and the analysis will determine which one, or what combination of potential delaminations will develop. The elements can also be

placed between every ply of a laminate, although it is not necessary to place them at interfaces between plies of the same orientations where delaminations occur rarely [19]. The cohesive behaviour assumes that failure of the elements is characterized by progressive degradation of the material stiffness, which is driven by a damage process. Delamination failures in composite laminates initiate and propagate under the combined influence of normal and shear stresses. The maximum nominal stress criterion is used for damage initiation. Delamination propagation is usually predicted by criteria established in terms of the energy release rates and fracture toughness under mixed-mode loading. This study is based on the power-law criterion proposed by Reeder [20]:

$$\left(\frac{G_I}{G_{IC}}\right)^n + \left(\frac{G_{II}}{G_{IIC}}\right)^n + \left(\frac{G_{III}}{G_{IIIC}}\right)^n = 1 \ , \qquad (1)$$

where G_I, G_{II}, and G_{III} are the energy release rates in modes I, II, and III, respectively, and G_{IC}, G_{IIC}, and G_{IIIC} are the corresponding critical energy release rates.

3.2.1. Discretization and mesh convergence

Presence of CZEs in the FE model defines the crack propagation path. The application of CZE requires a fine spatial discretization at the cohesive zone to capture the damage growth properly. Different models have been proposed in the literature to estimate the length of the cohesive zone, l_{cz} [6-8].This length is defined as the distance from the crack tip to the point where the final failure point is reached. The number of elements N_e in a cohesive zone according to [8], is given by

$$N_e = \frac{l_{cz}}{l_e} \ , \qquad (2)$$

where l_e is the mesh size in the direction of crack propagation. However, the minimum number of CZEs is not well established. Further, all these models are based on pre-existing and pre-defined cracks in the laminate such as in simulating tests of double cantilever beam (DCB) and mixed-mode bending (MMB) etc. tests. No accurate model is available to determine the cohesive element size for the FE model of the undamaged state before load application.

In this paper, the model proposed by Turon *et al.* [8] is used in the numerical analysis to obtain an initial estimate of the cohesive zone length and the interface element size defined by equation (2). Before performing further simulations, a mesh convergence study with different element lengths was performed and is summarized in figure 2. The results indicate that by decreasing the element length, the damage zone along the laminate length increases and solution convergence is achieved. Mesh 3 of 0.1 mm element length was selected for computationally effective simulations of multiple delaminations in numerical models A and B. A similar behaviour of CZE was also shown in [21], indicating that as long as the interface element size was taken less than 1 mm, numerical results were in agreement with experiments and a better solution convergence was achieved.

3.2.2. Stiffness of cohesive-zone elements

The interface element stiffness should be large enough to avoid relative displacements between the connected ply elements but also not too large to cause numerical problems such as spurious oscillations in interfacial traction of the cohesive element [8, 16, 21]. Several authors have proposed different methods to calibrate the cohesive element stiffness. Camanho *et al.* [7] obtained accurate results by using 10^6 N/mm^3 for graphite-epoxy specimens. Turon *et al.* [8] demonstrated that elastic properties of the composite would not be affected if the interface stiffness is defined as

$$K = \frac{\alpha E_{33}}{t_{\mathrm{p}}} \ , \qquad (3)$$

where E_{33} is the material's through-thickness stiffness, t_{p} is the thickness of ply connected by the cohesive element, and α is a non-dimensional parameter, which should be greater than 50 for accurate

simulation of various problems. Based on equation (3), the value of interface stiffness, $3x10^6$ N/mm^3 was used as a first estimate in this study. The stiffness was increased gradually until convergence was achieved at $8x10^6$ N/mm^3.

3.3. Boundary conditions and solution

Simply-supported boundary conditions are applied at the reference points of the rigid supports below the laminate representing the test fixture. A displacement-controlled load is applied at the centre rigid arc representing the indenter, which is in contact with the top ply of the laminate, for better convergence of the solution. Boundary conditions are applied at rigid surfaces instead of constraining the ply nodes as the local stresses due to the constraints edge effects disperse over greater distances of the structure because of the composite's anisotropy. As shown by Horgan *et al.* [22] for anisotropic composite materials, the application of St. Venant's principle for plane elasticity problems involving anisotropic materials is not justified in general. Quasi-static analysis is carried out for large-deflection effects by applying the load gradually in small time increments of 10^{-7} seconds to capture the damage process in the CZE. The final FE model B contained a total of 11,715 elements and it took 4 hours on a dual core machine with two 2.7 GHz processors each. The computational cost is a direct consequence of a fine mesh coupled with the highly nonlinear behaviour of interface damage elements.

4. X-ray tomography of the studied composite laminate

X-ray MicroCT measurements were performed using an XT H 225 X-ray scanner machine. The system consists of an X-ray detector and an electronic X-ray source, creating 2-dimensional cross-sections of the object. The source is a sealed X-ray tube operating at 25–225 kV with a 3 μm spot size. The specimen is positioned by an object manipulator with two translations and one rotation, rotating and raising/lowering the sample to a specific region of interest for adjustment of the sample magnification and acquisition of tomographic data. Following acquisition, a software program builds a precise 3D map from 2D radiograph images by 'stacking' the individual slices one on top of the other; this process is known as reconstruction. As denser materials absorb more X-rays than voids and air, this attenuation contrast allows detection and characterisation of cracks and flaws in the tomograpgic images.

High scan resolution is required to obtain maximum internal details of damage in the composite laminate. As the resolution is increased, the field of view of the sample is reduced. However, samples must remain within the field of view to obtain the radiographs of the region of interest, thus there is a trade off. A small sample of size 30 mm x 7 mm was prepared from the damaged region of the tested CFRP laminate to meet these requirements. Data for the sample was collected at 58 kV and 80 μA. Transmission X-ray images were acquired from 3600 rotation views over 360° of rotation (0.1° rotation step) for 3D reconstruction. These settings resulted in tomographs of 11 μm resolution as shown in figures 3 and 4.

5. Results and discussion

Numerical results of simulations of the large-deflection bending behaviour of CFRP laminates and comparison with experimental tests and MicroCT examination are presented in this section. The initiation and progression behaviours of multiple delaminations in model A is shown in figure 5. Damage is represented by a normalised length (L_d/L) of the cohesive layer along the beam axis against the normalised displacement loading (δ/δ_f), where δ_f is the displacement at the ultimate failure of the test specimen. Damage initiates faster in the overhang regions L (edge) of the top and mid cohesive layers than in the mid-regions L (mid). The overhang exhibits mode-I fracture whereas the mid-region is in mode-II state. However, delamination grows more rapidly in the MCL than TCL in the beam's mid-region until the MCL is completely damaged. This behaviour is more exaggerated in the results of multiple delaminations in model B shown in figures 6 and 7. Figure 6 demonstrates that although delamination initiates earlier in the beam's edges, it grows more in the mid-section. The MCL is more

damaged due to mode-II shear fracture as shown in figure 7. The reason for this is that the maximum through-thickness shear stresses generally occur in the mid-section of the laminate and drive the mode-II delamination process. Further, the mid-region exhibits mode-II delamination as shear stresses outside the beam's supports diminish and are maximum at the beam's neutral axis. In both numerical models, delamination initiates at above 30% of the failure load and then propagates at a higher rate. Damage suddenly spreads in correspondence with attainment of 70% of the failure load, especially in the middle section of the beam.

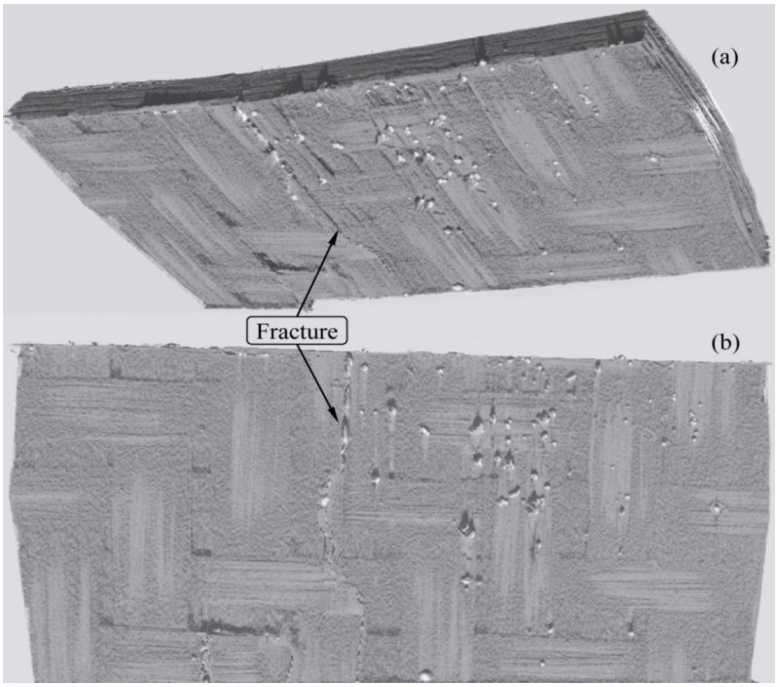

Figure 3. Ultimate fracture of 2 x 2 twill CFRP (resolution 11 μm): (a) Damage in three-dimensional volumetric reconstruction; (b) bottom surface

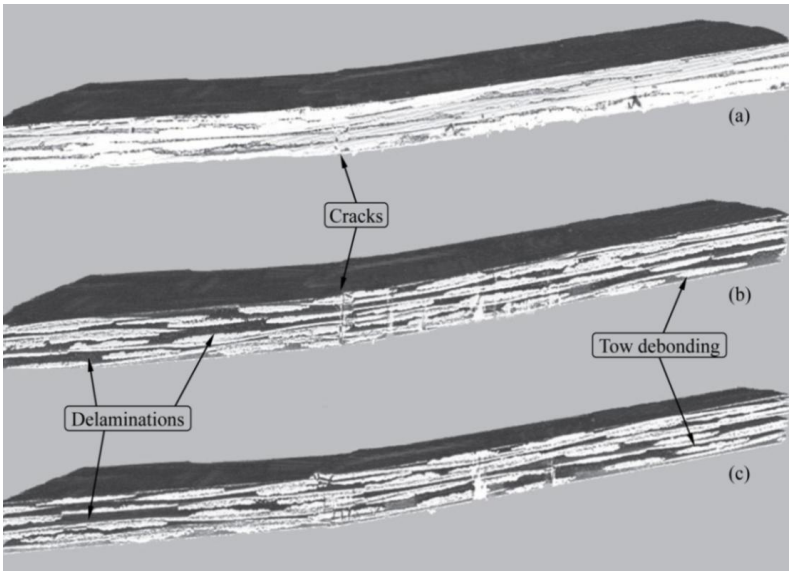

Figure 4. Damage mechanisms at various locations across the width of the sample (resolution 11 μm): (a) edge; (b) 50% of width; (c) 75% of the width

Comparison of the load-deflection behaviour obtained numerically for different models and experimentally from three-point bending tests of CFRP woven laminates is presented in figure 8. A good agreement is achieved between experiments and numerical simulations indicating that the numerical models are capable to reproduce the progressive failure of the laminate beams. It can be observed that the development of such interlaminar damage did not induce noticeable effects on the force *vs*. displacement curves till the stiffness degradation occur at points A, B and T. At these points the damage saturation occurs, followed by instantaneous loss of structure's load-carrying capability. Figure 8 shows that by increasing the number of cohesive layers in our FE models, the structure loses its load-carrying capability earlier and ultimate failure occurs at a lower load level.

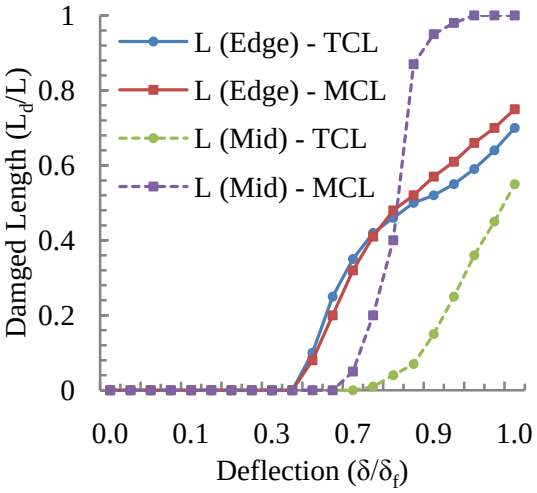

Figure 5. Damaged zone at edge and middle of beam - Model A

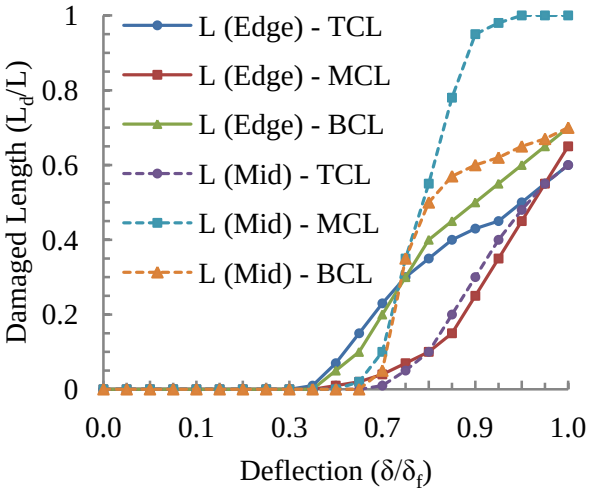

Figure 6. Damage zone at edge and middle of beam - Model B

The internal barely visible damage mechanisms are investigated with X-ray MicroCT. The 3D geometry of the ultimate transverse fracture and delamination in the laminate is shown in the volumetric reconstruction in figure 3. Figure 4 demonstrates damage in the resin-rich region between the plies of the sample at various locations across its width. Realisation of damage mechanisms at outer edge, 50% and 75% of the sample width is shown in figures 4a, b, and c respectively. It is shown that before ultimate fracture, the laminate exhibited microcraking and then delaminations and tow debondings. In the fibre-rich regions the damage is apparently associated with the debonding of the fibre/matrix interface. At the time of fracture, the internal structure shows that almost each ply was delaminated. Tow debonding also occurred because of the matrix cracking. All the tomographs show that the delamination is the prominent failure mode. The crack and damage is resolved based on the difference in the X-ray absorption between the carbon/epoxy material and air. Dark regions in images represent cracks and voids where as brighter regions represent the virgin material (see figure 4).

6. Conclusions

Damage in CFRP textile composites under large-deflection bending was studied using expeirmental tests, numerical simulations and MicroCT scanning. The tests were carried out to characterise the behaviour of the woven CFRP material. Two-dimensional plane-strain finite-element models were implemented in the commercial code Abaqus 6.10 using the explicit solver. A series of simulations was performed to study the onset and progression of inter-ply delamination process under mixed – mode large deflection bending by employing multiple layers of cohesive zone elements in the developed FE models. MicroCT images were obtained at 11 µm resolution to characterise the internal structural damage of the laminate.

The numerical results were quite close to the experimental ones, and the numerical models have the capability to reproduce the failure mechanisms in composite laminates. Numerical simulations showed that damage initiation and growth was sensitive to the mesh size of cohesive-zone elements. The results indicated the suitability of the developed numerical approach to study the onset and propagation of interlaminar damage. However, the calibration of numerical models based on interface layers proved to be highly mesh- and stiffness-sensitive and would certainly represent a critical issue

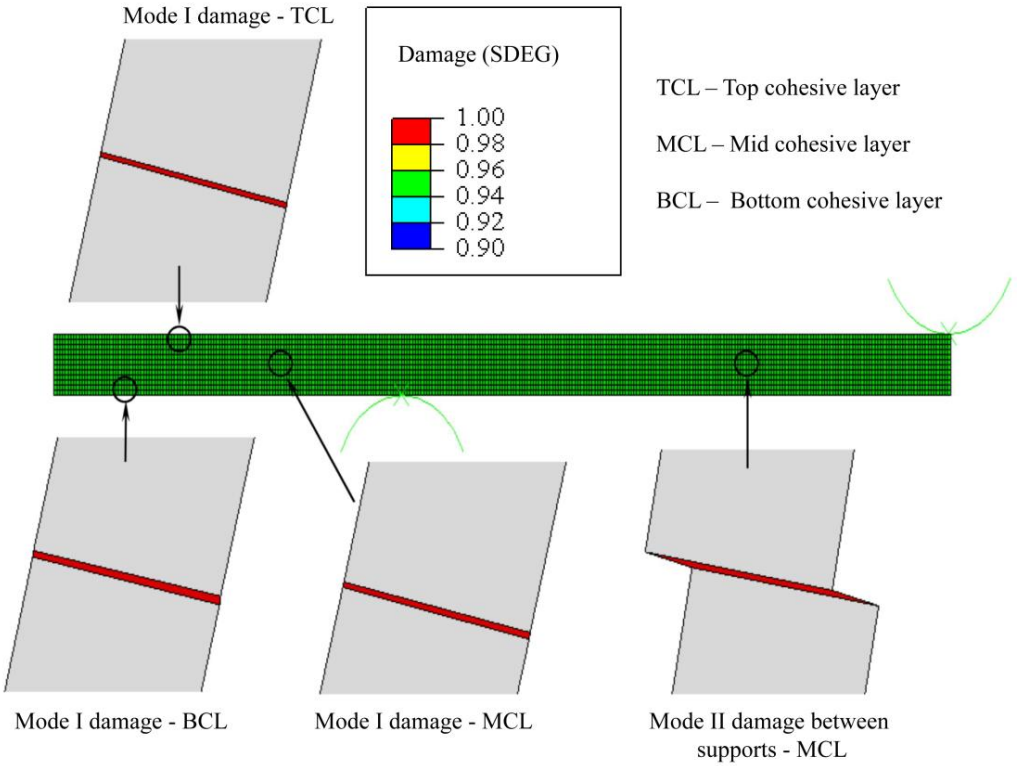

Figure 7. Development of interlaminar damage in multiple cohesive layers under bending

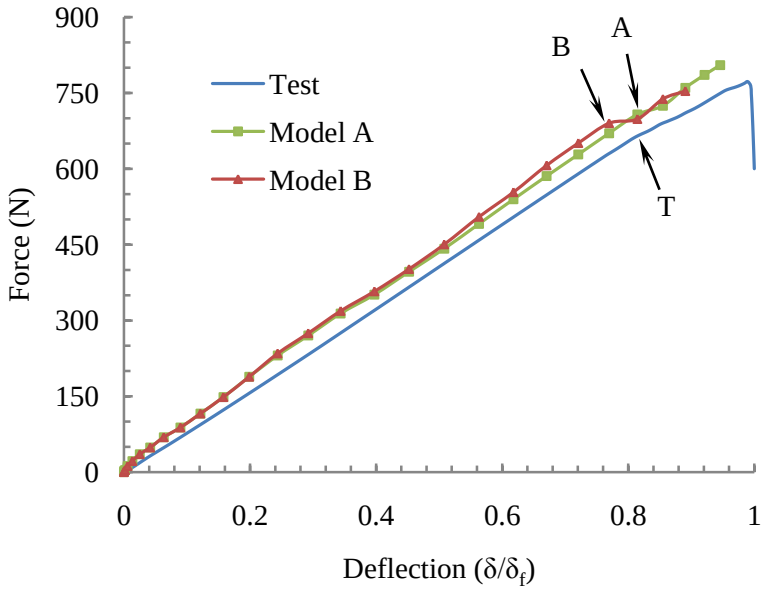

Figure 8. Numerical and experimental load-displacement response of CFRP laminates under bending

in the application of the approach to real-world components and structures. It is also important for all interface parameters to be calibrated and specified correctly in order to avoid long computational times, solution oscillations or even premature termination and to obtain better convergence. Therefore, a complete investigation of the mesh's sensitivity of the results, identification of the interface stiffness and strength levels through experiments, and a comparison of the results, obtained by applying different constitutive laws, are required to develop more reliable and robust 3D FE models.

X-ray MicroCT proved to be an excellent technique to investigate the internal failure behavior of composites. The detailed scans validated the behaviour of damage in finite element models. Three-dimensional reconstructions and subsequent cross-sectional images facilitated characterization of the location, type, size and geometry of damage in CFRP laminates. Based on the damage behaviour identified in the scanned images, three-dimensional detailed FE models are required to simulate interlaminar and intralaminar damage in woven composites, which will be addressed in the future work.

References

[1] C. Hochard, J. Payan, C. Bordreuil, International Journal of Fatigue, 28 (2006) 1270-1276.
[2] G. Ernst, M. Vogler, C. Hühne, R. Rolfes, Composites Science and Technology, 70 (2010) 6172.
[3] L. Iannucci, Computers & Structures, 84 (2006) 1029-1048.
[4] G. Wimmer, C. Schuecker, H.E. Pettermann, Composites Part B, 40 (2009) 158-165.
[5] G. Alfano, M.A. Crisfield, International Journal for Numerical Methods in Engineering, 50 (2001) 1701-1736.
[6] D.S. Dugdale, Journal of the Mechanics and Physics of Solids, 8 (1960) 100-104.
[7] P.P. Camanho, C.G. Davila, M.F. De Moura, Journal of Composite Materials, 37 (2003) 1415.
[8] A. Turon, C.G. Davila, P.P. Camanho, J. Costa, Engineering Fracture Mechanics, 74 (2007) 1665-1682.
[9] S.R. Stock, International Materials Reviews, 53 (2008) 129-181.
[10] P.J. Schilling, B.R. Karedla, A.K. Tatiparthi, M.A. Verges, P.D. Herrington, Composites Science and Technology, 65 (2005) 2071-2078.
[11] A.J. Moffat, P. Wright, J.Y. Buffière, I. Sinclair, S.M. Spearing, Scripta Materialia, 59 (2008) 1043-1046.
[12] P. Badel, E. Vidal-Sallé, E. Maire, P. Boisse, Composites Science and Technology, 68 (2008) 2433-2440.
[13] M.G. Andrews, R. Massabò, A. Cavicchi, B.N. Cox, International Journal of Solids and Structures, 46 (2009) 1815-1833.
[14] P. Lonetti, Computational Materials Science, 48 (2010) 563-575.
[15] C. Santiuste, S. Sánchez-Sáez, E. Barbero, Composite Structures, 92 (2010) 2406-2414.
[16] A. Airoldi, G. Sala, P. Bettini, Composites Science and Technology, doi:10.1016/j.compscitech.2009.10.011, 2009.
[17] F.P. Van Der Meer, L.J. Sluys, Journal of Composite Materials, 43 (2009) 2131.
[18] P. Feraboli, K.T. Kedward, Composites Part A, 34 (2003) 1265-1271.
[19] M.R. Wisnom, Composites Part A, 41 (2010) 795-805.
[20] J.R. Reeder, in: Technical Memorandum-1992-104210, NASA Langley Research Centre 1992.
[21] P. Naghipour, J. Schneider, M. Bartsch, J. Hausmann, H. Voggenreiter, Engineering Fracture Mechanics, 76 (2009) 2821-2833.
[22] C.O. Horgan, J.G. Simmonds, Composites Engineering, 4 (1994) 279-286.